Site-specific wave energy conversion performance of an oscillating water column device

I. López[a,*] , R. Carballo[a], G. Iglesias[b,c]

[a] *University of Santiago de Compostela, Hydraulic Engineering, Campus Universitario s/n, 27002, Lugo, Spain.*
[b] *MaREI, Environmental Research Institute & School of Engineering, University College Cork, College Road, Cork, Ireland.*
[c] *University of Plymouth, School of Engineering, Marine Building, Drakes Circus, Plymouth, PL4 8AA, United Kingdom.*

Abstract

The energy conversion performance of oscillating water column (OWC) wave energy converters at a specific site is often studied by means of analytical models. Based on linear theory, these models lose accuracy when viscous losses and turbulence become significant—more generally, when nonlinear effects play a role, as they often do in real operating conditions. In this work we apply a novel methodology based on a combination of numerical modelling and laboratory tests to investigate OWC performance without these shortcomings. First, high-resolution wave resource characterisation matrices are obtained by means of numerical modelling. Second, the resource matrices are combined with the OWC efficiency matrices obtained through laboratory tests and, importantly, including the effects of turbine-induced damping and air compressibility—usually disregarded in small-scale laboratory tests, but relevant for full-size (prototype) devices. The combined matrices thus obtained express, through a wave height-period distribution, the energy captured by the OWC for different values of the damping coefficient. On this basis, developers can select the most appropriate value of turbine-induced damping for a given site, based on performance values. The implementation of the novel methodology is illustrated through a case study in Galicia (NW Spain), in which three deployment sites are considered. We find that the turbine-induced damping must be matched to the wave climate of the site for an OWC device to achieve high performance; indeed, changes in damping cause variations in the total annual energy captured of up to 11%, which increase to 25% for specific sea states.

Keywords

wave energy; characterisation matrices; OWC; air compressibility; physical modelling; capture width ratio

* Corresponding author
e-mail address: ivan.lopez@usc.es (I. López)

1. Introduction

Nowadays, renewable energies have become a pillar for energy sustainability, and constitute an essential element in reducing greenhouse gas emissions (Gacitua *et al.*, 2018). In an effort to enhance the role of renewables in the energy mix, the exploitation of novel renewable energy sources, such as marine renewable energies, has focused the attention of the scientific community over the last decades. In this context, wave energy is particularly promising thanks to its high resource availability (Weiss *et al.*, 2018), low impact (Atan *et al.*, 2019; Özkan-Haller *et al.*, 2017), good predictability (Carballo and Iglesias, 2012; Veigas *et al.*, 2015) and multiple synergies with other marine renewables (Astariz, Perez-Collazo *et al.*, 2015; Astariz, Abanades *et al.*, 2015). The exploitation of the wave resource, however, is challenging given the large variability in waves and, in particular, the large extreme-average ratios. As a result, the development of efficient, flexible, and reliable wave energy converter technologies is very much the focus of intense research at the moment.

Among the variety of wave energy converters under development (e.g., Di Fresco and Traverso, 2014; Oliveira *et al.*, 2016; Rodríguez *et al.*, 2018), oscillating water column (OWC) devices (Falcão and Henriques, 2016) stand out for their simplicity. The only mechanical element (an air turbine) is located at the top of an empty chamber, therefore not in direct contact with salt water. The chamber is connected to the sea through an underwater opening, so it is partially filled with water. Wave action causes the oscillation of the water column inside the chamber and, consequently, the alternating compression and decompression of the air trapped above the free surface. The pressure difference between the interior of the chamber and the atmosphere generates an air flow which drives the turbine. A specific turbine design is required, capable of maintaining a unidirectional rotation under the alternating flow. Axial-flow reaction (also known as Wells) turbines and self-rectifying impulse turbines are the most common alternatives (Falcão *et al.*, 2018).

The performance of both elements, turbine and chamber, is closely related. In fact, among the parameters that most influence the performance of an OWC wave energy converter, the damping exerted by the turbine on the oscillations of the water column was found to be one of the most important parameters, if not the most important (López, Castro *et al.*, 2015; López, Pereiras *et al.*, 2015). Therefore, it is essential that the influence of the turbine be taken into account from the earlier stages of the design. The fact that the turbine-induced damping affects the performance of the system implies that the efficiency of an OWC, even at a hydrodynamic level (before considering the mechanical efficiency of the turbine), cannot be defined by a single power matrix: there should be a

different power matrix for each value of the turbine-induced damping (López *et al.*, 2016). Thus, the structural simplicity of the converter contrasts with the complexity of its operating mode.

The hydrodynamic modelling of OWC wave energy converters has been mostly carried out by means of analytical models based on linear potential flow theory (e.g., Malara, Giovanni and Arena, 2013; Rezanejad *et al.*, 2015; Zheng *et al.*, 2018), resorting to numerical methods for dealing with complex geometries (Brito-Melo *et al.*, 2001; Malara, G. *et al.*, 2017). These models are inadequate for non-small waves and non-linear effects such as viscous losses and turbulence, which are important under real operating conditions. Therefore, the performance analysis of an OWC at a site requires advanced techniques considering these effects, such as experimental modelling. Over the last few years, experimental modelling has been used in the hydrodynamic modelling of OWC converters to evaluate the performance of different geometric parameters of the chamber (Ning *et al.*, 2016; Vyzikas *et al.*, 2017), to analyse the efficiency of an array of OWC devices integrated into an offshore detached breakwater (Ashlin *et al.*, 2018), to analyse the enhancement that harbour walls induce on the performance of the system (Raj *et al.*, 2019), or to measure the wave loads on the front and rear walls of the OWC for structural design purposes (Pawitan *et al.*, 2019; Viviano *et al.*, 2016).

Experimental modelling is based on dimensional analysis techniques that relate the conditions in a small-scale model (typically between 1:100 and 1:10 scale) to those on a full-size prototype. Thus, to correctly emulate the real conditions in the model is of paramount importance to avoid substantial errors in model predictions. An important aspect when experimentally modelling an OWC is the spring-like effect of the air inside the chamber, which despite it being usually disregarded, is known to be significant at full-size OWC converters (Falcão and Henriques, 2014; Falcão and Henriques, 2016); in fact, such effects were not taken into account in none of the aforementioned experimental works. In effect, it has been found that if air compressibility is not considered, significant errors are introduced in the assessment of the OWC efficiency, resulting in both under- and over-predictions depending on the wave conditions and the turbine-induced damping (Falcão and Henriques, 2014).

In this work, the site-specific energy conversion performance of an OWC device was evaluated following a methodology that involves an accurate assessment of the available wave energy resource at the locations of interest and the thorough computation of the efficiency of the OWC device. The latter was determined through an extensive experimental campaign in which non-linear effects—with special emphasis on the spring-like effect of air compressibility—, together with three different values of the turbine-induced damping—representative of three turbines of different characteristics—were

taken into account. Rather than testing the sea states of the locations of interest, a more general approach was followed. A comprehensive set of sea states were tested comprising all the possible combinations of wave period and wave height within the operational limits of the converter. The idea behind this approach is to fully characterise the OWC for deployment at whatever location. The performance of the OWC was measured based on: (i) the capture width ratio—the percentage of the incident wave energy that is captured by the OWC in the form of pneumatic energy per width of device—and (ii) the total energy captured in a year, which is ultimately the most important factor. The methodology was illustrated through a case study in Galicia (Spain), considering three study sites.

The paper is structured as follows. In Section 2, the foundations of the developed methodology are described. It is subdivided in three parts: (i) characterisation of the wave energy resource through numerical modelling; (ii) characterisation of the OWC performance though physical model tests; and (iii) calculation of the energy capture of the device. In Section 3 the results at the three study sites, expressed in terms of the OWC efficiency matrices and the energy captured matrices, are described. Finally, conclusions are drawn in Section 4.

2. Materials and methods

2.1. Wave resource characterisation

The wave energy resource at each site of interest is characterised by means of the WEDGE (Wave Energy Diagram Generator) procedure (Carballo, Sánchez, Ramos, Taveira-Pinto *et al.*, 2014; Carballo, Sánchez, Ramos and Castro, 2014). This procedure is based on the *energy bin* concept (Iglesias and Carballo, 2010), i.e., a trivariate interval of significant wave height (H_{m0}), energy period (T_e) and mean wave direction (θ_m) of a certain size, allowing the reconstruction of high-resolution characterisation matrices at each site of interest, so that most of the exploitable resource is accounted for. The first step of the methodology consists in characterising the offshore energy resource along the Galician coast. For this purpose, three buoys (Silleiro, Vilán Sisargas, and Bares buoys) (Figure 1) representative of the deepwater wave climate in Galicia are used, covering approx. a 15-year period of hourly seas states, which leads to an accurate description of its deepwater wave climate. At these buoys, the most energetic bins, with a resolution of 0.5 m of H_{m0} and 0.5 s of T_e—the largest resolution of WECs' efficiency currently available—and 22.5º of θ_m, are determined. With this in view, each sea state is assigned to its corresponding bin and its wave power per unit with (J) determined as:

$$J = \frac{\rho_w g}{16} H_{m0}^2 C_g \ , \tag{1}$$

where ρ_w is the water density; g is the gravitational acceleration; and C_g is the group velocity obtained as:

$$C_g = \frac{1}{2}\left(1 + \frac{2kh}{\sinh(2kh)}\right)\left(\frac{gT_e}{2\pi}\tanh(kh)\right) , \tag{2}$$

where k is the wave number and h the water depth. So, the total energy provided by each bin (E_w) is determined as:

$$E_w = J\,O_b \ , \tag{3}$$

where O_b is the occurrence of the sea states within each energy bin, expressed in hours.

Then, the most energetic bins contributing to 95% of the total available resource at each buoy are retained for further analysis, i.e., 720, 787, 693 bins in the case of Silleiro, Vilán-Sisargas and Bares buoys, respectively, which in turn represent virtually 100% of the exploitable resource. After that, the selected energy bins are propagated towards the sites of interest through high-resolution spectral numerical models. This is conducted by implementing three different models, each of them forced with its corresponding deepwater dataset, and validated against nearshore wave records (Carballo, Sánchez, Ramos, Taveira-Pinto *et al.*, 2014). The model results are H_{m0}, T_e, and θ_m at each grid node along with other spectral information, and the resulting wave power computed as:

$$J = \rho_w g \int_0^{2\pi}\int_0^{\infty} S(f,\theta) C_g(f)\, df\, d\theta \ , \tag{4}$$

where $S(f,\theta)$ is the spectral energy density. The information made available combined with the computed occurrence of the propagated conditions (the occurrence is conserved through the propagation process) can be used to reconstruct site-specific high-resolution characterisation matrices. As a result, the efficiency matrices of OWC converters can be combined with the resulting resource information to determine any performance parameter of specific OWC-site combinations.

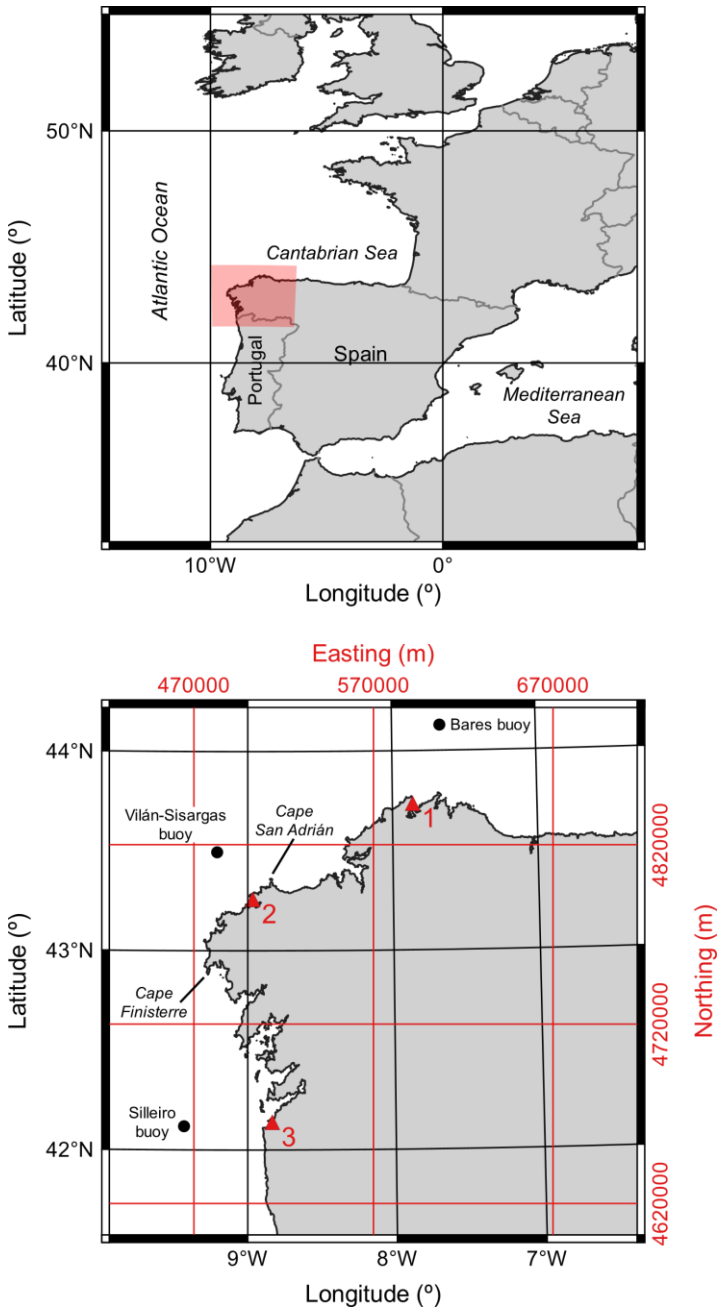

Figure 1. Locations of the three study sites in Galicia (NW Spain).

2.1.1. Selection of study sites

In order to illustrate the methodology proposed, three sites in the Galician nearshore of interest for installing an OWC converter were selected (NW Spain). The location of the three selected sites, Cariño (1), Corme (2) and Panxón (3), is presented in Figure 1 and their UTM coordinates and depth are included in Table 1.

Table 1. Easting (*X*) and northing (*Y*) coordinates (UTM29N/ETRS89) and water depth (*h*) of the three study sites.

Study site	***X***	***Y***	***h***
Cariño (1)	591770 m	4843092 m	12.7 m
Corme (2)	502782 m	4789545 m	12.0 m
Panxón (3)	513645 m	4665291 m	10.1 m

The three sites correspond to small to medium ports that are suitable for the installation of a breakwater-integrated OWC thanks to their characteristics—mainly, bathymetry and wave exposure. Furthermore, in an attempt to represent different wave energy distributions, the study sites cover different geographic areas: site 1, the North coast of Galicia; site 2, the so-called Death Coast (*Costa da Morte*), extending from Cape Finisterre to Cape San Adrián (Figure 1); and site 3, the Southwest coast or *Rías Baixas*.

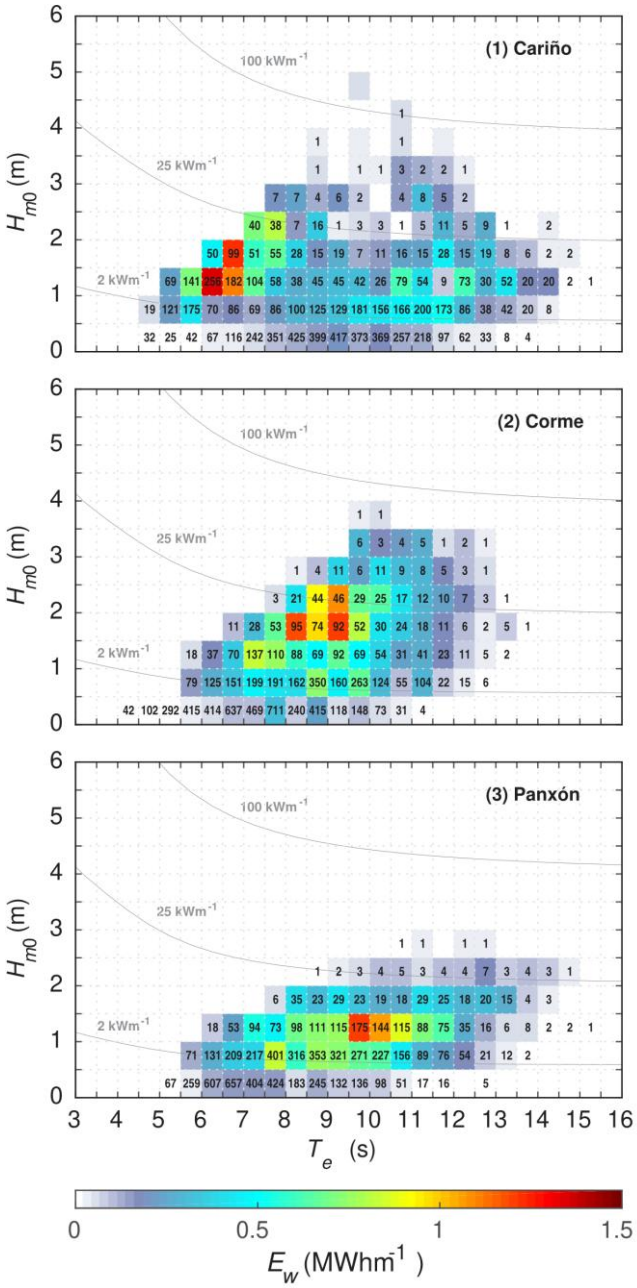

159

160 Figure 2. Wave resource characterisation matrices in an average year for the three selected study sites.
161 The colour scale represents the total energy per metre of wave front (E_w) provided by each energy bin;
162 the numbers indicate the occurrence of the sea states within each energy bin, expressed in hours; and
163 the isolines provide the wave power.

164 The wave resource characterisation matrices of these three study sites are presented in Figure 2.
165 The matrices were discretised in bins of 0.5 s (ΔT_e) × 0.5 m (ΔH_{m0}). The three locations present a
166 moderate wave climate, with values of the total energy per metre of wave front in an average year of
167 27.14, 27.06 and 21.49 MWhm^{-1}, for Cariño (1), Corme (2) and Panxón (3), respectively. Despite
168 these rather similar average values, the wave resource distribution across energy periods is markedly
169 different at the three sites. At site 1 most of the energy is provided by sea states with energy periods

between 6 and 8 s; at site 2, the energy is concentrated in energy periods between 8 and 10 s; finally, at site 3, the bulk of the energy is supplied by sea states with energy periods between 9.5 and 11 s. This is likely due to the fetch increasing from site 1, which is exposed to the Bay of Biscay, to site 3, exposed to the North Atlantic Ocean. Regarding the resource distribution across significant wave heights, the most energetic sea states correspond with wave heights between 1.0 and 2.5 m at the three study sites, with a slight deviation towards the lower values in the case of site 3.

2.2. OWC performance characterisation

2.2.1. Physical modelling

The physical model represents, at a 1:25 scale ratio, a standard design of breakwater-integrated OWC wave energy converter (Figure 3a). Taking into account that the construction costs are one of the main downsides of OWC technology, multi-purpose solutions constitute an interesting and more feasible approach. With this as background, a breakwater-integrated OWC enables both coastal protection and energy harnessing by means of a sole structure, thereby maximising the benefits and minimising the costs. The OWC model tested in this work (Figure 3b) is two-dimensional, its width matching that of the wave flume. The model and prototype dimensions are presented in Table 2.

As previously mentioned, the damping exerted by the turbine on the water column oscillation is one of the most important factors, if not the most important one, affecting the efficiency of an OWC converter. Therefore, modelling the turbine-induced damping is a prerequisite for obtaining reliable results. In this work, the turbine-induced damping was modelled through an orifice (e.g., Perez-Collazo *et al.*, 2018; Vyzikas *et al.*, 2017), i.e., an element introducing a pressure drop which varies quadratically with the flow rate, and therefore appropriately reproducing the behaviour of a self-rectifying impulse turbine (Falcão and Henriques, 2016). In comparison to Wells turbines, impulse turbines present a series of characteristics that make them particularly interesting for breakwater-integrated OWC converters: smaller diameter, lower rotational speed and consequently lower levels of noise. In addition, impulse turbines present a smoother efficiency curve, i.e., a good performance over a broader range of flow conditions. Three different orifices of diameter D = 28, 31 and 39 mm were tested, corresponding to opening ratios (ratio of the orifice area to the plan area of the OWC chamber) of 0.8%, 1.0% and 1.5%, respectively. The three orifices are representative of three impulse turbines of different diameter—for self-rectifying impulse turbines, the relationship between pressure drop and flow rate is not significantly affected by changes in rotational speed (Falcão and Henriques, 2014).

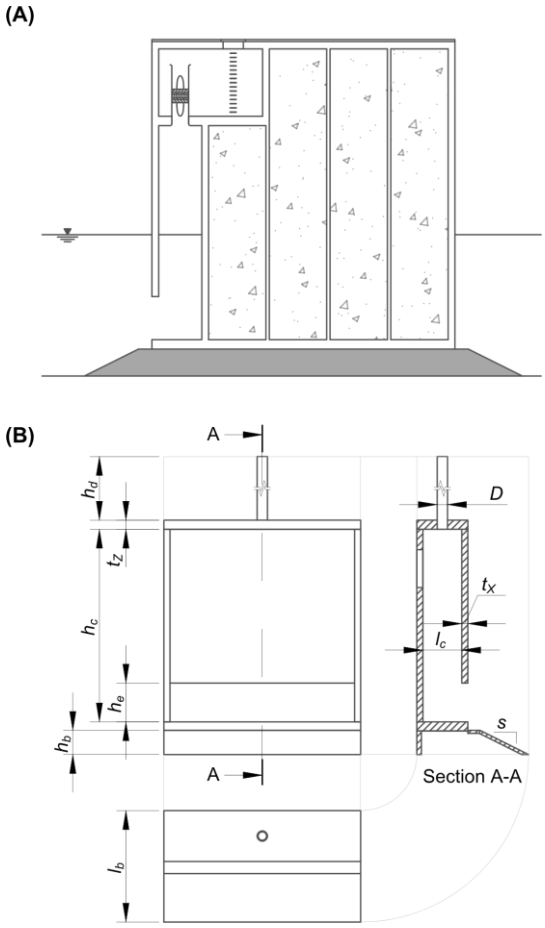

Figure 3. Sketch of a breakwater-integrated OWC (A) and views of the tested OWC converter (B).

Table 2. Dimensions of the geometrical parameters of the OWC converter.

Geometrical parameter	**Symbol**	**Model dimensions**	**Prototype dimensions**
Chamber height	h_c	63.6 cm	15.9 m
Chamber length (in the wave direction)	l_c	12.8 cm	3.2 m
Entrance height	h_e	12.8 cm	3.2 m
Vertical walls thickness	t_Z	2.0 cm	0.5 m
Horizontal walls thickness	t_X	2.8 cm	0.7 m
Orifice diameter	D	Variable	—
Duct height	h_d	25D	—
Bedding height	h_b	8.0 cm	2.0 m
Bedding length	l_b	20.0 cm	5.0 m
Bedding slope	s	1:2	1:2

The scaling of the model was based on Froude's similitude, i.e., equal ratio of inertia to gravity forces between model and prototype. This is a mandatory assumption when dealing with free surface flows (Hughes, 1993). However, in the case of OWC wave energy converters, the spring-like effect of the air inside the chamber is known to play an important role, which calls for maintaining also an equal ratio of inertia to air compression forces between model and prototype (Weber, 2007). To this end the air chamber volume must be scaled according to (Falcão and Henriques, 2014):

$$\frac{V_m}{V_p} = \frac{n_m}{n_p}\lambda^{-2}\delta^{-1}\,, \tag{5}$$

where the subscripts *m* and *p* refer to model and prototype, respectively; V is the volume of the air chamber; n is the polytropic exponent of the turbine, which takes the values $n_p = 1.2$ and $n_m = 1.0$ for a full-size turbine and for an orifice, respectively; λ is the scale factor ($\lambda = 25$); and δ is the water density ratio (ρ_m/ρ_p), which takes a value of $\delta = 0.98$ for wave flume testing.

The approach to meeting both aforementioned requirements is to apply the Froude similitude criterion and perfect geometric similarity in the hydrodynamic domain (wet part of the model) but considering a distorted aerodynamic domain (upper part of the chamber) that fulfils Eq. (5). The required volume was achieved by connecting the air chamber to a rigid-walled air reservoir of an adequate volume (Figure 5). This is the procedure recommended for OWC small-scale modelling as stated by Falcão and Henriques (2014). By applying Eq. (5), the volume of the air chamber at model scale should be $V_m = 538.4$ dm^3, which makes it necessary to add to the chamber a volume of 513.2 dm^3.

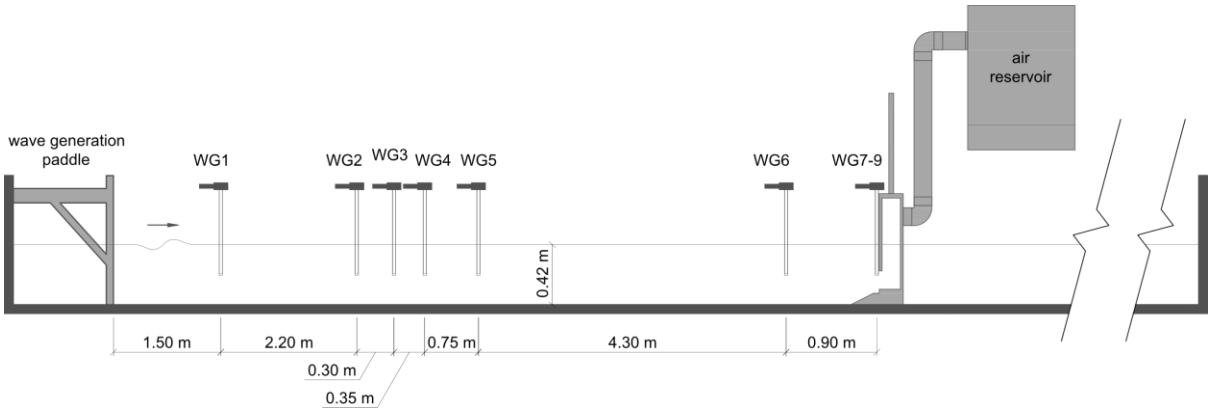

Figure 4. Experimental set-up of the model OWC.

Physical model tests were carried out in the wave flume of the University of Santiago de Compostela (USC), with dimensions of 20 m × 0.65 m in plan view. It is equipped with a piston paddle wave generation system with active absorption of the reflected waves. The experimental set-up is presented in Figure 4. A total of nine wave gauges were installed to monitor the wave propagation, analyse the incident and reflected wave field, and check the absence of transverse waves. Additionally, two ultrasonic level sensors were placed inside the chamber to measure the oscillations of the water column. Finally, a differential pressure sensor registered the time-varying pressure drop between the atmosphere and the interior of the chamber.

The experimental campaign comprised 49 irregular wave conditions (Figure 5), representative of as many omnidirectional *energy bins* (Carballo, Sánchez, Ramos and Castro, 2014), or bivariate intervals that discretise the sea states according to their H_{m0} and T_e. Thus, all the sea states with a significant wave height and an energy period within the range of an energy bin are assumed to be represented by a single capture width ratio—corresponding to the wave conditions representative of the energy bin. The smaller the size of the energy bins, the greater the precision of the performance matrix. In this work, an interval size of 1.0 m for significant wave height and 1.0 s for energy period were used.

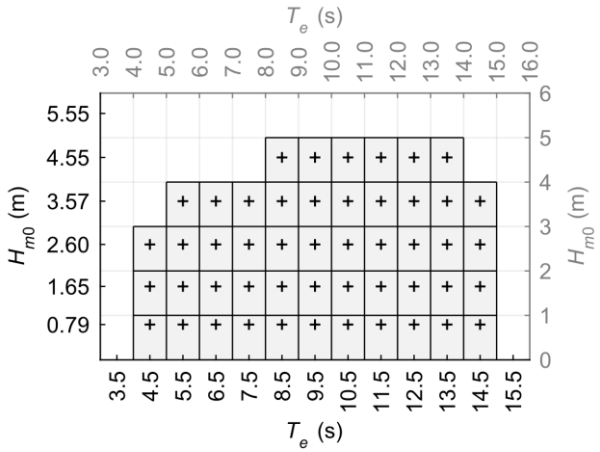

Figure 5. Sea states covered in the experimental campaign. The grey axes represent the boundaries of the sea states and the black axes the representative wave conditions tested. The crosses indicate the representative wave condition of each energy bin.

The selection of the representative wave conditions of each energy bin is, therefore, of paramount importance. As wave energy varies linearly with energy period, the representative energy period was set to the arithmetic mean of the energy periods at the limits of the bin. However, wave energy varies quadratically with the significant wave height, so the representative value should provide the mean wave energy of the bin, satisfying the following equation:

$$\int_{H_1}^{H_R} H^2 dH = \int_{H_R}^{H_2} H^2 dH \ , \tag{6}$$

where H_1 and H_2 are the wave height at the limits of each bin; and H_R is the representative value of the wave height of that bin (Carballo, Sánchez, Ramos, Taveira-Pinto *et al.*, 2014).

The 49 selected bins cover energy periods from 4 to 15 s and wave heights from 0 to 5 m (limit established based on the characteristics of the OWC). For the selected study sites the 49 bins cover more than 99% of the energy and time of the wave resource matrices presented in Figure 2 for the three study sites.

In order to experimentally test the representative wave conditions, it is necessary to assign to each of them a wave energy frequency distribution, i.e., a frequency spectral density function or wave spectrum. The wave spectrum better representing the wave conditions at the region of interest is the JONSWAP spectrum (Carballo *et al.*, 2015), that is given by the form (Hasselmann *et al.*, 1973):

$$S_J(f) = \alpha g^2 (2\pi)^{-4} f^{-5} \exp\left(-\frac{5}{4}\left(\frac{f}{f_p}\right)^{-4}\right) \gamma^{\exp\left(-\frac{1}{2}\left(\frac{f/f_p - 1}{\sigma}\right)^2\right)}, \quad (7)$$

where α is a scaling parameter, f_p is the peak frequency (the reciprocal of the peak period), γ is the peak enhancement factor and σ is a spectral shape parameter that takes the following values:

$$\sigma = \begin{cases} 0.07 & for\ f < f_p \\ 0.09 & for\ f \geq f_p \end{cases}. \quad (8)$$

The scaling parameter α was adjusted in order to obtain, through numerical integration of the spectrum, the desired value of the significant wave height for each wave condition. For the peak enhancement factor, based on previous works at the same location (Arean *et al.*, 2017), a value of γ = 3.3 was selected. The peak period of each wave condition was calculated from the energy periods defined in Figure 5, using the ratio:

$$\frac{T_e}{T_p} = 0.90, \quad (9)$$

which corresponds to JONSWAP-type spectra with a peak enhancement factor of 3.3 (Goda, 2010).

Each of the 49 irregular wave conditions was tested for the three orifice diameters—in total, 147 irregular wave tests were conducted. Testing times vary depending on the period of each wave condition in order to ensure that, at least, 200 waves were generated, a number large enough to decrease the sampling variation of the wave statistics (Goda, 2010).

2.2.2. Calculation of the efficiency matrices

The performance of the OWC under the wave conditions representative of each energy bin was characterised based on the capture width ratio (also known as relative capture width), which reflects the fraction of the wave power flowing through the device that is absorbed by the device (Babarit, 2015), defined by

$$C_{WR} = \frac{P_p}{P_w w}, \quad (10)$$

where P_p is the mean pneumatic power absorbed by the OWC; P_w is the mean available wave power per unit width of wave front; and w is the width of the OWC chamber (transverse to wave direction). The mean pneumatic power is defined as

$$P_p = \frac{1}{t_{max}} \int_0^{t_{max}} \Delta p \, Q \, dt \ , \tag{11}$$

where t_{max} is the time duration of each test; Δp is the pressure drop directly measured by the differential pressure sensor; and Q is the air flow rate through the orifice calculated as

$$Q = \mathrm{sgn}(\Delta p) \left(\frac{B_r}{|\Delta p|} \right)^{1/2} \ , \tag{12}$$

being B_r a damping parameter which represents the pressure-flowrate relationship for each orifice, obtained in the present case through numerical and physical modelling following the definition as provided by López *et al*. (2015):

$$B^* = \frac{\Delta p^{1/2}}{Q} \frac{A_c}{\rho_a^{1/2}} = B_r^{1/2} \frac{A_c}{\rho_a^{1/2}} \ , \tag{13}$$

where A_c is the water plane area of the OWC chamber ($A_c = l_c \times w$); and ρ_a is the air density. For the three orifice diameters, D = 28, 31 and 39 mm, these parameters take the values $B_r = 5.30 \times 10^6$, 3.59×10^6 and 1.48×10^6 kg/m^7 (in model dimensions) and B^* = 160.49, 132.18 and 84.85, respectively.

The mean wave power per unit width of wave front is given by

$$P_w = \rho_w g \int_0^\infty S(f) \, C_g(f) \, df \ , \tag{14}$$

where $S(f)$ is the incident spectral energy density; and $C_g(f)$ is the group velocity of each frequency band.

2.3. Energy capture

Finally, the pneumatic energy captured by the OWC for the three values of the turbine-induced damping at the three study sites was calculated. First, the pneumatic power captured by each i-th energy bin ($E_{p,\,i}$) was obtained following:

$$E_{p,\,i} = C_{WR,\,i} \, E_{w,\,i} \ . \tag{15}$$

where $C_{WR,\,i}$ and $E_{w,\,i}$ are the capture width ratio and the available wave energy of each i-th energy bin, respectively. As there are three efficiency matrices—one for each value of turbine-induced damping—

and three wave resource characterisation matrices—one for each study site—there will be nine different energy capture matrices.

Second, the total annual available energy and the total annual captured energy was calculated, respectively, as:

$$E_{w,\,annual} = \sum_{i=1}^{N} E_{w,\,i} \quad , \tag{16}$$

$$E_{p,\,annual} = \sum_{i=1}^{N} E_{p,\,i} \quad , \tag{17}$$

where N is the number of energy bins of each matrix. Last, the annual capture width ratio was calculated as:

$$C_{WR,\,annual} = \frac{E_{p,\,annual}}{E_{w,\,annual}} \quad . \tag{18}$$

3. Results

3.1. OWC efficiency matrices

The efficiency matrices of the OWC wave energy converter, obtained through the experimental campaign, are presented in Figure 6 for the three values of the turbine-induced damping, i.e., for three turbines with different diameter. Incidentally, a methodology to dimension the turbine diameter from the values of the damping coefficient was developed by Pereiras *et al.* (2015). The efficiency matrices are expressed in terms of the C_{WR}; this term is preferred over the absorbed power because, as a relative indicator, it removes the bias that would otherwise result from the fact that wave power is proportional to the square of the wave height.

The comparison between the three graphs shows a clear influence of the turbine-induced damping on the performance of the device: for individual energy bins there are variations in the C_{WR} of up to 40% depending on the value of the damping coefficient (e.g., 0 m < H_{m0} < 1 m, 5 s < T_e < 6 s). However, given that the greater differences in the values of the C_{WR} are apparent only for the less powerful sea states (those with the lower values of wave height and small periods), it is expected that the overall influence of the turbine-induced damping on the energy captured by the OWC be lower.

The optimum value of the damping coefficient varies depending on the wave conditions. Thus, for sea states with small wave period (T_e < 9 s) and low wave height (H_{m0} < 3 m), the value of the damping coefficient that provides the higher values of C_{WR} is B^* = 84.85; in the case of sea states with larger periods (T_e > 9 s) the value of the damping coefficient that provides the best efficiency is the

medium one (B^* = 132.18), or the largest one (B^* = 160.49) if the wave height is very low (H_{m0} < 1 m).

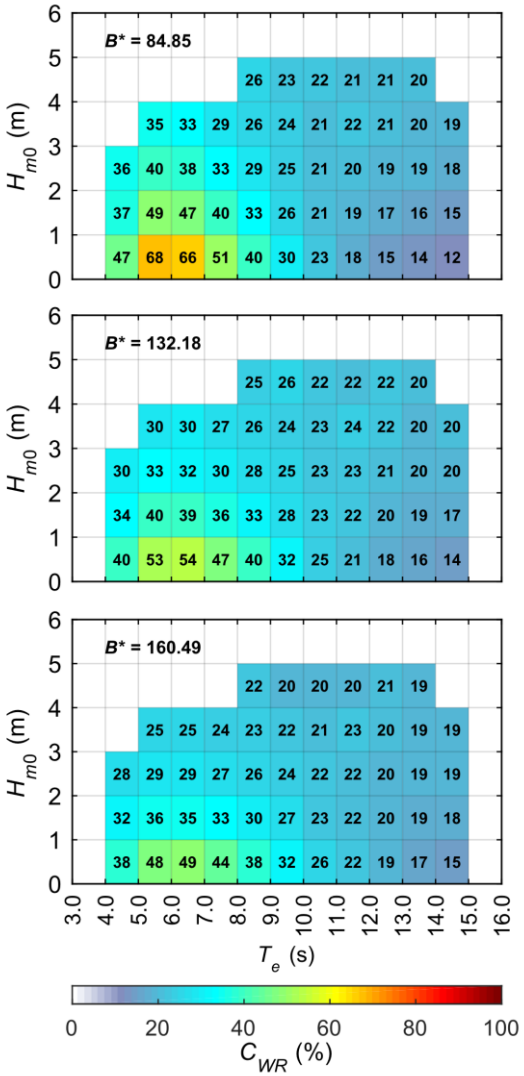

Figure 6. Efficiency matrices of the OWC wave energy converter expressed in terms of the capture width ratio (C_{WR}), given as a percentage, for the three values of the damping coefficient tested (for further clarification, the numeric value is also included).

The variation of C_{WR} amongst energy bins presents a similar distribution for the three values of the damping coefficient: a band of higher efficiency for sea states with energy period between 5 s and 7 s, that decreases as wave height increases. Although the resonant period (that for which the C_{WR} is maximum) slightly increases when the damping coefficient increases, from 5 s < T_e < 6 s for B^* = 84.85 to 6 s < T_e < 7 s for B^* = 132.18 and 160.49, the change is minimal and, for the studied range of damping values, does not enable an adjustment of the resonant period of the OWC by modifying the turbine-induced damping.

The efficiency matrices presented in Figure 6 characterise the OWC and, therefore, can be used to evaluate the pneumatic power production of the device in whatever location (with the limitation of having a similar water depth).

3.2. Energy captured by the OWC

The captured pneumatic energy matrices of the OWC are presented in Figure 7. These matrices are obtained by combining (energy bin by energy bin) the efficiency matrices of the OWC (Figure 6) with the wave resource characterisation matrices at the three study sites (Figure 2).

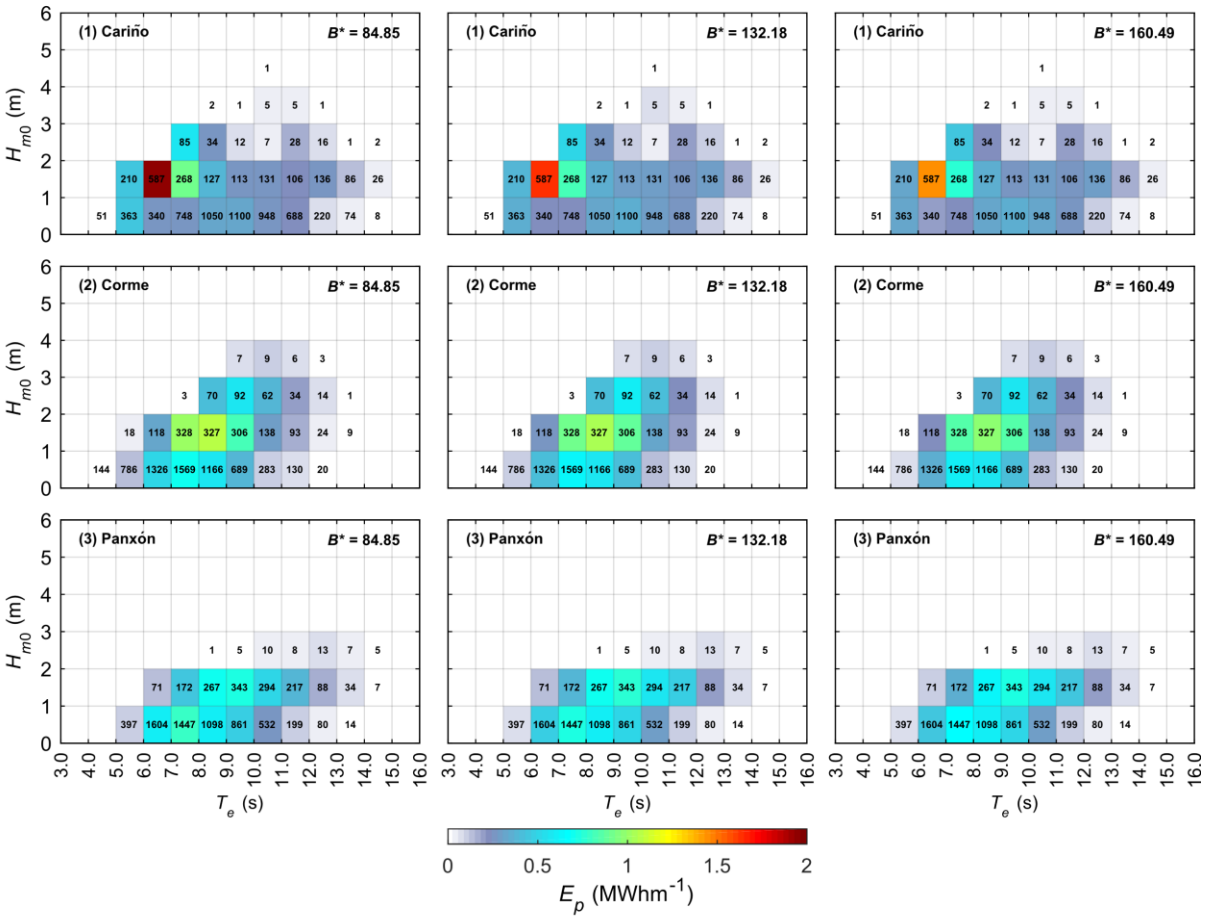

Figure 7. Captured energy matrices of the OWC per unit width of converter for the three values of the damping coefficient (B^*), at the three study sites. The colour scale represents the total pneumatic energy per metre of wave front (E_p) captured by the OWC in each energy bin; the numbers indicate the occurrence of the sea states in that energy bin, expressed in hours.

Comparing the results of annual captured energy (for whichever study site and value of the damping coefficient) with the efficiency matrix of the corresponding damping coefficient (Figure 6), it can be seen that energy bins with higher values of capture width ratio (those that comprise sea states

with energy period between 5 s and 7 s and low wave height) do not provide the bulk of captured energy; in contrast, the variable that determines which energy bins provide the greatest amount of captured energy is the available wave energy as provided by the site-specific characterisation matrices (Figure 2). Thus, the energy bins providing the greatest amount of captured energy vary depending on the study site: at site 1, they correspond to sea states with energy periods between 6 and 7 s; at site 2, to sea states with periods between 8 and 9 s; and, finally, at site 3, to sea states with periods between 9 and 10 s. In the three cases, the energy bin that provides the largest captured energy comprises sea states with a significant wave height between 1 and 2 m, which in turn correspond to those providing the bulk of the wave energy resource (Section 2.1.1).

The influence of the turbine-induced damping is also noticeable. For example, at study site 1, the bin providing the greatest amount of captured energy (6 s < T_e < 7 s, 1 m < H_{m0} < 2 m) with a total of 1.96 MWhm^{-1} for the lowest damping (B* = 84.85) and 1.47 MWhm^{-1} for the largest one (B* = 160.49), which implies a reduction of more than 25% in the captured energy. Notwithstanding, the energy bin that provides the greatest amount of captured energy is the same (6 s < T_e < 7 s, 1 m < H_{m0} < 2 m) for the three values of the damping coefficient. At study site 2, the energy bin providing the largest amount of captured energy (in this case 8 s < T_e < 9 s, 1 m < H_{m0} < 2 m) is again the same for the three values of the damping coefficient. However, at study site 3 the bin allowing the greatest energy production differs depending on the turbine-induced damping considered: in the case of B* = 132.18 and 160.49 it corresponds to the interval delimited by 9 s < T_e < 10 s and 1 m < H_{m0} < 2 m, and for B* = 84.85 to the interval delimited by 7 s < T_e < 8 s and 0 m < H_{m0} < 1 m.

The results of the total annual available energy ($E_{w,\,annual}$) and the total annual captured energy ($E_{p,\,annual}$), together with the annual capture width ratio ($C_{WR,\,annual}$), are presented in Figure 8. The study site that provides the greatest amount of captured energy is Cariño (study site 1) with 8.7 MWhm^{-1} and an annual capture width ratio of 32.1%. At this location, the value of that damping coefficient that performs best is the lowest (B* = 84.85). Although site 1 presents a level of total annual available energy equivalent to site 2 (27.14 vs 27.06 MWhm^{-1}, respectively), the total annual captured energy in the former is greater. This is due to the fact that site 1 corresponds to the location in which sea states of shorter energy periods (T_e < 8 s) provide more energy (Figure 2), which in turn are those with the largest efficiency (Figure 6). Therefore, an accurate wave resource characterisation in the form of highly discretised wave-height-vs-energy-period matrix is of paramount importance for assessing the energy production of an OWC wave energy converter.

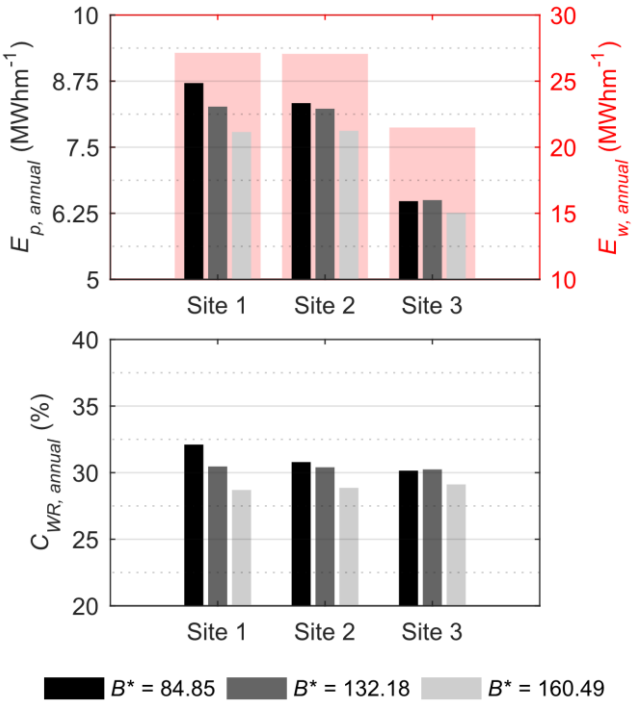

Figure 8. Comparison of the annual energy conversion performance of the OWC per unit width of converter for the three values of the damping coefficient (B^*), at the three study sites, expressed in terms of the total annual captured pneumatic energy (top graph, left axis) and of the annual capture width ratio (bottom graph). For reference, the total annual available wave energy is also represented in the top graph (right axis).

A wrong selection of the damping coefficient would reduce the total annual captured energy by 5% and 11% for the medium and largest values of the damping coefficient, respectively, which would have repercussions for the profitability of a wave farm. Furthermore, in this work in particular, there are two aspects that contribute to decrease the impact of the turbine-induced damping on the total annual captured energy: (i) the three values of the damping coefficient were chosen based on previous works (e.g., López *et al.*, 2016), so they present similar values, close to the overall optimum turbine-induced damping of the chamber; and (ii) as indicated above, the greater differences in the values of the C_{WR} correspond to sea states with short periods (Figure 6) which, for the study sites considered, do not provide the bulk of energy (Figure 2). This situation, though, may be different in other locations.

Interestingly, the value of the damping coefficient that provides the greater performance in the study site 3 is the medium one (B^* = 132.18). The lowest damping, which provides the largest amount of energy production at study sites 1 and 2, descends to the second position in study site 3. Additionally, in the case of analysing the most appropriate location for a given turbine, it is found that for a turbine with damping coefficient B^* = 84.85 or B^* = 132.18 the best location corresponds to

study site 1, and for a turbine with a value of damping coefficient B^* = 160.49, study site 2 emerges as the most appropriate one. This great variability points out the importance of correctly matching the turbine-induced damping and the wave conditions that affect the OWC. It follows that an accurate site-specific wave resource characterisation in the form of high-resolution characterisation matrices is the first step towards a meaningful performance evaluation of an OWC wave energy converter.

Finally, the similarity between the annual captured width ratio at the three study sites (Figure 8 – bottom) does not lead to similar values in the total annual captured energy (in particular, comparing study site 3 with 1 and 2). This difference in the total annual captured energy is mainly connected to the occurrence of the sea states in an energy bin, that varies substantially from one study site to another (Figure 7) and emphasises, again, the importance of an accurate characterisation of the available wave energy resource.

4. Conclusions

In this work, a comprehensive methodology to accurately evaluate the site-specific performance of an OWC wave energy converter considering the turbine-induced damping together with usually disregarded non-linear effects—in particular, the spring-like effect of air compressibility—is presented. Thus, the novelty of this work lies not only in the results achieved but also in the methodology presented, which constitutes an outcome on its own. The methodology is illustrated through a case study in Galicia (NW Spain) in which three locations of interest are considered for installing OWC technology.

The methodology is based on a combination of physical and numerical modelling. First, high-resolution characterisation matrices considering virtually 100% of the exploitable resource are computed at each site by implementing novel procedures based on the energy bin concept. Second, small-scale physical model tests, in which air compressibility is appropriately considered, are carried out to determine the efficiency matrices of the OWC for three different values of the turbine-induced damping (i.e., three impulse turbines of different diameter); irregular wave conditions representative of each energy bin were simulated, covering the virtual totality (> 99%) of the wave energy resource in the characterisation matrices. Finally, resource and efficiency matrices were combined to obtain the captured energy matrices that express, through a bivariate discretisation, the pneumatic energy that the OWC captures for each turbine-induced damping at each site.

The methodology enables the selection of the most appropriate site and turbine-induced damping combination based on performance values: of the three study sites considered, Cariño (1), Corme (2) and Panxón (3), the best performance was attained at study site 1 with a total annual captured energy of 8.7 $MWhm^{-1}$ and an annual capture width ratio of 32.1%; the value of the damping coefficient that performs best at this site was the lowest of those considered (B^* = 84.85). Moreover, the selection of the best turbine for a given location is also possible: the value of the damping coefficient providing the best performance at site 2 is also the lowest; unlike at site 3, where the medium value (B^* = 132.18) yields the best results. Finally, the best site for a specific turbine can be also selected: the best site for B^* = 84.85 and B^* = 132.18 was found to be site 1, and for B^* = 160.49, site 2. Going beyond the methodology itself, the results showed that considering the turbine-induced damping is of paramount importance in maximising the energy captured by an OWC device: when damping coefficients changes, variations in the total annual energy captured of up to 11% were found, which increase to 25% for individual energy bins. Furthermore, there is not a single optimum value of turbine-induced damping for all sea states; indeed, the optimum depends on both the energy period and the significant wave height. It follows that an accurate highly-discretised characterisation of the wave energy resource is necessary. In addition, it was found that it is neither the capture width ratio nor the power of the incoming sea states but the available wave energy provided by the site-specific characterisation matrices that determines principally which energy bins provide the greatest amount of annual captured energy, which highlights again the importance of the resource characterisation stage.

To sum up, the methodology presented in this work allows the accurate assessment of the performance of an OWC wave energy converter at a specific coastal site, considering a highly-discretised resource characterisation, non-linear effects, air compressibility effects and several levels of turbine-induced damping. It constitutes the first step towards a wave-to-wire model in which non-linear effects are thoroughly taken into account, with special emphasis on the influence of air compressibility.

Acknowledgements

During this work I. López was supported by the postdoctoral grant ED481B 2016/125-0 of the 'Programa de Axudas á etapa posdoutoral da Xunta de Galicia (Consellería de Cultura, Educación e Ordenación Universitaria)'.

References

Arean, N., Carballo, R., Iglesias, G., 2017. An integrated approach for the installation of a wave farm. Energy 138, 910-919. https://doi.org/10.1016/j.energy.2017.07.114.

Ashlin, J., Sannasiraj, S.A., Sundar, V., 2018. Performance of an array of oscillating water column devices integrated with an offshore detached breakwater. Ocean Eng. 163, 518-532. https://doi.org/10.1016/j.oceaneng.2018.05.043.

Astariz, S., Abanades, J., Perez-Collazo, C., Iglesias, G., 2015. Improving wind farm accessibility for operation & maintenance through a co-located wave farm: Influence of layout and wave climate. Energy Conv.Manag. 95, 229-241. https://doi.org/10.1016/j.enconman.2015.02.040.

Astariz, S., Perez-Collazo, C., Abanades, J., Iglesias, G., 2015. Co-located wind-wave farm synergies (Operation & Maintenance): A case study. Energy Conv.Manag. 91, 63-75. https://doi.org/10.1016/j.enconman.2014.11.060.

Atan, R., Finnegan, W., Nash, S., Goggins, J., 2019. The effect of arrays of wave energy converters on the nearshore wave climate. Renew.Energy 172, 373-384. https://doi.org/10.1016/j.oceaneng.2018.11.043.

Babarit, A., 2015. A database of capture width ratio of wave energy converters. Renew.Energy 80, 610-628. https://doi.org/10.1016/j.renene.2015.02.049.

Brito-Melo, A., Hofmann, T., Sarmento, A J N A, Clément, A.H., Delhommeau, G., 2001. Numerical modelling of OWC-shoreline devices including the effect of surrounding coastline and non-flat bottom. Int.J.Offshore Polar Eng. 11 (2), 147-154.

Carballo, R., Iglesias, G., 2012. A methodology to determine the power performance of wave energy converters at a particular coastal location. Energy Conv.Manag. 61, 8-18. https://dx.doi.org/10.1016/j.enconman.2012.03.008.

Carballo, R., Sánchez, M., Ramos, V., Castro, A., 2014. A tool for combined WEC-site selection throughout a coastal region: Rias Baixas, NW Spain. Appl.Energy 135, 11-19. https://dx.doi.org/10.1016/j.apenergy.2014.08.068.

Carballo, R., Sánchez, M., Ramos, V., Fraguela, J.A., Iglesias, G., 2015. Intra-annual wave resource characterization for energy exploitation: A new decision-aid tool. Energy Conv.Manag. 93, 1-8. https://doi.org/10.1016/j.enconman.2014.12.068.

Carballo, R., Sánchez, M., Ramos, V., Taveira-Pinto, F., Iglesias, G., 2014. A high resolution geospatial database for wave energy exploitation. Energy 68, 572-583. https://dx.doi.org/10.1016/j.energy.2014.02.093.

Di Fresco, L., Traverso, A., 2014. Energy conversion of orbital motions in gravitational waves: Simulation and test of the Seaspoon wave energy converter. Energy Conv.Manag. 86, 1164-1172. https://doi.org/10.1016/j.enconman.2014.06.048.

Falcão, A.F.O., Henriques, J.C.C., 2014. Model-prototype similarity of oscillating-water-column wave energy converters. Int.J.Mar.Energy 6, 18-34. https://dx.doi.org/10.1016/j.ijome.2014.05.002.

511 Falcão, A.F.O., Henriques, J.C.C., 2016. Oscillating-water-column wave energy converters and air
512 turbines: A review. Renew.Energy 85, 1391-1424.
513 https://dx.doi.org/10.1016/j.renene.2015.07.086.

514 Falcão, A.F.O., Henriques, J.C.C., Gato, L.M.C., 2018. Self-rectifying air turbines for wave energy
515 conversion: A comparative analysis. Renew.Sust.Energ.Rev. 91, 1231-1241.
516 https://doi.org/10.1016/j.rser.2018.04.019.

517 Gacitua, L., Gallegos, P., Henriquez-Auba, R., Lorca, Á, Negrete-Pincetic, M., Olivares, D., et al.,
518 2018. A comprehensive review on expansion planning: Models and tools for energy policy
519 analysis. Renew.Sust.Energ.Rev. 98, 346-360. https://doi.org/10.1016/j.rser.2018.08.043.

520 Goda, Y., 2010. Random Seas and Design of Maritime Structures: Third Edition. World Scientific
521 Publishing, Singapore.

522 Hasselmann, K., Barnett, T.P., Bouws, E., Carlson, H., Cartwright, D.E., Enke, K., et al., 1973.
523 Measurements of wind-wave growth and swell decay during the Joint North Sea Wave Project
524 (JONSWAP). Ergnzungsheft zur Deutschen Hydrographischen Zeitschrift Reihe A(8), 12.

525 Hughes, S.A., 1993. Physical models and laboratory techniques in coastal engineering. World
526 Scientific, Singapore.

527 Iglesias, G., Carballo, R., 2010. Wave power for La Isla Bonita. Energy 35 (12), 5013-5021.
528 https:10.1016/j.energy.2010.08.020.

529 López, I., Castro, A., Iglesias, G., 2015. Hydrodynamic performance of an oscillating water column
530 wave energy converter by means of particle imaging velocimetry. Energy 83, 89-103.
531 https://dx.doi.org/10.1016/j.energy.2015.01.119.

532 López, I., Pereiras, B., Castro, F., Iglesias, G., 2015. Performance of OWC wave energy converters:
533 influence of turbine damping and tidal variability. Int.J.Energy Res. 39 (4), 472-483.
534 https://doi.org/10.1002/er.3239.

535 López, I., Pereiras, B., Castro, F., Iglesias, G., 2016. Holistic performance analysis and turbine-
536 induced damping for an OWC wave energy converter. Renew.Energy 85, 1155-1163.
537 https://dx.doi.org/10.1016/j.renene.2015.07.075.

538 Malara, G., Gomes, R.P.F., Arena, F., Henriques, J.C.C., Gato, L.M.C., Falcão, A.F.O., 2017. The
539 influence of three-dimensional effects on the performance of U-type oscillating water column
540 wave energy harvesters. Renew.Energy 111, 506-522.
541 https://doi.org/10.1016/j.renene.2017.04.038.

542 Malara, G., Arena, F., 2013. Analytical modelling of an U-Oscillating Water Column and
543 performance in random waves. Renew.Energy 60, 116-126.
544 https://dx.doi.org/10.1016/j.renene.2013.04.016.

545 Ning, D., Wang, R., Zou, Q., Teng, B., 2016. An experimental investigation of hydrodynamics of a
546 fixed OWC Wave Energy Converter. Appl.Energy 168, 636-648.
547 https://doi.org/10.1016/j.apenergy.2016.01.107.

548 Oliveira, P., Taveira-Pinto, F., Morais, T., Rosa-Santos, P., 2016. Experimental evaluation of the
549 effect of wave focusing walls on the performance of the Sea-wave Slot-cone Generator. Energy
550 Conv.Manag. 110, 165-175. https://doi.org/10.1016/j.enconman.2015.11.071.

Özkan-Haller, H.T., Haller, M.C., McNatt, J.C., Porter, A., Lenee-Bluhm, P., 2017. Analyses of Wave Scattering and Absorption Produced by WEC Arrays: Physical/Numerical Experiments and Model Assessment. In: Z. Yang, Copping A (Eds.), Marine Renewable Energy: Resource Characterization and Physical Effects, Springer International Publishing, Cham, pp. 71-97. https://doi.org/10.1007/978-3-319-53536-4_3.

Pawitan, K.A., Dimakopoulos, A.S., Vicinanza, D., Allsop, W., Bruce, T., 2019. A loading model for an OWC caisson based upon large-scale measurements. Coast.Eng. 145, 1-20. https://doi.org/10.1016/j.coastaleng.2018.12.004.

Pereiras, B., López, I., Castro, F., Iglesias, G., 2015. Non-dimensional analysis for matching an impulse turbine to an OWC (oscillating water column) with an optimum energy transfer. Energy 87, 481-489. https://dx.doi.org/10.1016/j.energy.2015.05.018.

Perez-Collazo, C., Greaves, D., Iglesias, G., 2018. Hydrodynamic response of the WEC sub-system of a novel hybrid wind-wave energy converter. Energy Conv.Manag. 171, 307-325. https://doi.org/10.1016/j.enconman.2018.05.090.

Raj, D., Sundar, V., Sannasiraj, S.A., 2019. Enhancement of hydrodynamic performance of an Oscillating Water Column with harbour walls. Renew.Energy 132, 142-156. https://doi.org/10.1016/j.renene.2018.07.089.

Rezanejad, K., Bhattacharjee, J., Guedes Soares, C., 2015. Analytical and numerical study of dual-chamber oscillating water columns on stepped bottom. Renew.Energy 75, 272-282. https://dx.doi.org/10.1016/j.renene.2014.09.050.

Rodríguez, C.A., Rosa-Santos, P., Taveira-Pinto, F., 2018. Assessment of the power conversion of wave energy converters based on experimental tests. Energy Conv.Manag. 173, 692-703. https://doi.org/10.1016/j.enconman.2018.08.009.

Veigas, M., López, M., Romillo, P., Carballo, R., Castro, A., Iglesias, G., 2015. A proposed wave farm on the Galician coast. Energy Conv.Manag. 99, 102-111. https://doi.org/10.1016/j.enconman.2015.04.033.

Viviano, A., Naty, S., Foti, E., Bruce, T., Allsop, W., Vicinanza, D., 2016. Large-scale experiments on the behaviour of a generalised Oscillating Water Column under random waves. Renew.Energy 99, 875-887. https://doi.org/10.1016/j.renene.2016.07.067.

Vyzikas, T., Deshoulières, S., Barton, M., Giroux, O., Greaves, D., Simmonds, D., 2017. Experimental investigation of different geometries of fixed oscillating water column devices. Renew.Energy 104, 248-258. https://doi.org/10.1016/j.renene.2016.11.061.

Weber, J., 2007. Representation of non-linear aero-thermodynamic effects during small scale physical modelling of OWC WECs. 7th European Wave and Tidal Energy Conference, Porto, Portugal, pp. 11-14.

Weiss, C.V.C., Guanche, R., Ondiviela, B., Castellanos, O.F., Juanes, J., 2018. Marine renewable energy potential: A global perspective for offshore wind and wave exploitation. Energy Conv.Manag. 177, 43-54. https://doi.org/10.1016/j.enconman.2018.09.059.

Zheng, S., Zhang, Y., Iglesias, G., 2018. Wave–structure interaction in hybrid wave farms. J.Fluids Struct. 83, 386-412. https://doi.org/10.1016/j.jfluidstructs.2018.09.012.